Journal of Orthopaedic Translation 24 (2020) 103–111

Contents lists available at ScienceDirect

Journal of Orthopaedic Translation

journal homepage: www.journals.elsevier.com/journal-of-orthopaedic-translation

ORIGINAL ARTICLE

Biomechanical, histologic, and molecular characteristics of graft-tunnel healing in a murine modified ACL reconstruction model

Huan Yu [a,b], Fangda Fu [a], Sai Yao [a], Huan Luo [e], Taotao Xu [a,b], Hongting Jin [a,b], Peijian Tong [a,b], Di Chen [b,d], Chengliang Wu [a,b,**], Hongfeng Ruan [a,b,c,*]

[a] Institute of Orthopaedics and Traumatology, The First Affiliated Hospital of Zhejiang Chinese Medical University, Hangzhou 310053, Zhejiang Province, China
[b] First Clinical College of Zhejiang Chinese Medical University, Hangzhou 310053, Zhejiang Province, China
[c] Longhua Hospital Affiliated to Shanghai University of Traditional Chinese Medicine, Shanghai 200032, China
[d] Research Center for Human Tissues and Organs Degeneration, Shenzhen Institutes of Advanced Technology, Chinese Academy of Sciences, Shenzhen 518055, China
[e] Department of Pharmacy, The Second Affiliated Hospital, Zhejiang University School of Medicine, Hangzhou 310009, China

ARTICLE INFO

Keywords:
Anterior cruciate ligament
Hedgehog signaling
Mouse model
Tendon-bone healing

SUMMARY

Purpose: The purpose of our study was to introduce and validate a metal-free, reproducible and reliable mouse model of anterior cruciate ligament (ACL) reconstruction (ACLR) surgery as an effective tool for a better understanding of molecular mechanisms of graft-tunnel healing after ACLR.

Methods: A total of 150 C57BL/6 mice were randomly allocated into five Groups: Group 1 (mice with intact ACL), Group 2–4 (mice underwent modified ACLR surgery and sacrificed 1-, 2-, and 4-weeks after surgery), and Group 5 (mice underwent unmodified ACLR surgery and sacrificed 4 weeks after surgery). Micro-computed tomography (CT), biomechanical histological as well as immunohistochemical (IHC) analyses were performed to characterize the modified ACLR.

Results: Micro-CT analysis demonstrated there is a non-significant increase in BV/TV and BMD of the bone tunnel during the tendon-to-bone healing following ACLR. Biomechanical tests showed that the mean load-to-failure forces of Group 3 and 4 are equal to 31.7% and 46.0% of that in Group 1, while the stiffness was 33.1% and 57.2% of that of Group 1, respectively. And no obvious difference in biomechanical parameters was found between Group 4 and 5. Histological analysis demonstrated that formation of fibrovascular tissue in the tibial tunnel and aperture in Groups 4 and 5 and direct junction appeared between tendon graft and tunnel both in Groups 4 and 5. IHC results showed that there are gradually enhanced expression of Patched1, Smoothened and Gli2 concomitant with decreased Gli3 protein in the tendon-bone interface during the tendon-bone healing process.

Conclusion: We introduced a metal-free, reproducible and reliable mouse model of ACLR compared to the unmodified ACLR procedure, and characterized the expression pattern of key molecules in Ihh signaling during the graft healing process.

The translational potential of this article: In the present study we introduced and validated, for the first time, a metal-free, reproducible and reliable ACLR mouse model, which could be used to investigate the detailed molecular mechanisms of graft-tunnel healing after ACLR. We also explored new strategies to promote the healing of tendon-to-bone integration.

Abbreviations: ACL, Anterior cruciate ligament; ACLR, ACL reconstruction; BMD, Bone mineral density; BV/TV, Bone volume/total volume; CT, Computed tomography; H&E, Haematoxylin-eosin; NS, Non-significant; Ihh, Indian hedgehog; Ptch1, Patched1; Smo, Smoothened; Gli1, Glioma-associated oncogene homologue 1; Gli2, Glioma-associated oncogene homologue 2; Gli3, Glioma-associated oncogene homologue 3; CI, Confidence interval.

* Corresponding author. Institute of Orthopaedics and Traumatology, The First Affiliated Hospital of Zhejiang Chinese Medical University, Hangzhou 310053, Zhejiang Province, China.

** Corresponding author. Institute of Orthopaedics and Traumatology, The First Affiliated Hospital of Zhejiang Chinese Medical University, Hangzhou 310053, Zhejiang Province, China.

E-mail addresses: wcl@zcmu.edu.cn (C. Wu), rhf@zcmu.edu.cn (H. Ruan).

https://doi.org/10.1016/j.jot.2020.05.004
Received 5 October 2019; Received in revised form 15 May 2020; Accepted 20 May 2020
Available online 2 June 2020

Introduction

Anterior cruciate ligament (ACL) tear is one of the most prevalent sports-related injuries, which can lead to devastating consequences. Epidemiological studies showed that approximately 250, 000 patients undergo this procedure annually in the United States with a lifetime cost of US $ 8 billion [1,2]. In order to restore athletic ability before the injury as much as possible, ACL reconstruction (ACLR) is the most commonly performed ligamental replacement surgery [2–4]. However, this surgical management results in more than 20% risk of structural and mechanical failure at the surgical site [3,5,6]. Moreover, 40% of individuals receiving the ACLR surgery exhibited reduced mobility and quality of life [6–9]. Therefore, it is a great challenge to further improve postoperative outcomes of ACLR surgery.

It is well known that a firm tendon graft-to-bone attachment is pivotal to the functional substitutes of the graft. Both large animal and clinical studies showed that low quality of fibrovascular tissue interface forms via a scar-mediated process between tendon graft and bone tunnel [10–12]. And this slow and incomplete graft-tunnel healing process, which fails to recapitulate the structure and corresponding function of the native ligament, led to a prolonged period of rehabilitation and more vulnerable to post-surgery complication such as graft laxity, tunnel widening [13]. This dilemma urges us to uncover the enigma in physiology and molecular mechanisms of graft healing, which may provide novel insights for developing effective strategies to optimize and accelerate healing progression.

Mouse models that mimic human diseases are important tools for investigating the underlying mechanisms in various diseases and the development of new therapeutic strategies for human pathology. Toward this end, mice model of ACLR should be developed so that the role of specific genes or cellular signaling on tendon-bone healing could be applied to transgenic strain. The latest research by Deng *et al* [14] developed a novel murine ACLR model using a clip for femoral suspensory fixation and transosseous suture for tibial fixation. Based on their murine model, we modified their murine model of ACLR in C57BL/6 background. The novelty of our model was that we provide a metal-free, reproductive and liable method to reconstruct the ACL of mice.

Hedgehog (Hh) signaling pathway is an evolutionarily conserved developmental cassette from Drosophila to humans, participating in development, homeostasis and skeletal repair [16]. The Hh ligands consist of Indian hedgehog (Ihh), Sonic hedgehog (Shh), and Desert hedgehog (Dhh). In the absence of Hh ligands, patched 1 (Ptch1) receptor represses smoothened (Smo) activity, and the Gli transcription factors (Gli2 and Gli3) are proteolytically cleaved into repressors to suppress downstream genes [16]. Binding of Hh ligands to Ptch1 relieves its inhibition of Smo, which activates Gli-dependent downstream targets. Gli2 generally acts as an activator rather than a repressor of GLI-mediated transcription, while Gli3 mainly presents as the repressor form [16]. Previous studies have revealed that the Ihh is the main Hh ligand in growth plate and required for endochondral bone formation. Hh signaling pathway also plays a critical role in enthesis growth, fibrocartilage differentiation, and calcified cartilaginous mineralization [17,18]. Another work on scarring and regeneration of murine skin would healing confirmed that dermal activation of Hh pathway reinstalls a regenerative dermal niche, making wound healing be redirected to promote hair follicle regeneration instead of fibrotic repair [19]. However, it has been given much less attention to the effects of key proteins in Hh signaling on scar-mediated fibrovascular formation in murine tendon-bone healing.

Hence, the main purpose of the present work was to develop a modified ACLR model applied to mice, which has comparable biological and biomechanical changes to those of the previous murine ACLR model established by Deng *et al* [14]. Moreover, we further characterized key proteins in Hh signaling during the process of graft-tunnel healing.

Materials and methods

Animals

Eight-week-old male C57BL/6J mice were provided by the Experimental Animal Research Center of Zhejiang Chinese Medical University. All mice were fed in specific pathogen-free animal facilities and free access to water and lab chow. The room was maintained at a controlled temperature (23 ± 2°C) and humidity (40 ± 5%). All procedures were approved by the Animal Experimentation Ethics Committee of Zhejiang Chinese Medical University (ZSLL-2018-40). Both the ARRIVE (Animals in Research: Reporting *In Vivo* Experiments) guidelines for reporting animal research [20] and Guide for the Care and Use of Laboratory Animal (1996) [21] were carried out.

Experimental design

A total of 150 mice were randomly allocated into five Groups: Group 1 (mice with intact ACL), Group 2–5 (mice underwent primary ACLR or modified ACLR surgery). The mice in Group 2, 3 and 4 underwent a modified ACLR surgery with a soft-tissue sling fixation on the femoral side and sacrificed respectively at 1, 2 and 4 weeks after surgery, while the mice in Group 5 underwent the primary ACLR surgery described by Deng *et al* [14] and sacrificed at 4 weeks after surgery. Histology, immunohistochemistry (IHC) analysis, micro-CT analysis and biomechanical tests were further performed according to the experimental flow shown in Fig. 1.

Surgical procedure of modified ACLR and primary ALCR

All surgeries were performed by an orthopedic surgeon engaged in arthroscopy and sports medicine. After proper anesthesia (0.5% pentobarbital sodium, 0.15 mL/10 g body weight) and sterilization, mice were maintained in the supine position. Ahead of bone tunnel drilling, femoral footprint targeting was performed via simulation to identify the very orientation of the drilling needle. Before native ACL was cut off, the femoral tunnel was drilled using a 25-gauge needle (diameter = 0.5 mm) from ACL femoral footprint to the lateral aspect of the femoral condyle, while the tibial tunnel was drilled under direct vision from the medial tibia outside the footprint of ACL tibial insertion with a 25G needle (Fig. 2A and B). Following two small longitudinal incisions on the medial ankle and sole of foot, the flexor digitorum longus was identified and separated (Fig. 2C and D). With a high tense suture (Ethicon 7-0) placed at its distal end, the tendons were harvested and preserved in PBS. Utilizing a 1-cm skin incision over the ipsilateral front knee and lateral parapatellar approach, the patella was subluxated medially and the tibial insertion of the ACL was exposed with the knee flexed. Under the traction of the attached suture, the tendon graft was pulled through the tibial and femoral tunnels in turn (Fig. 2E). A needle was used to probe the lateral head of gastrocnemius from the posterior aspect of the lateral collateral ligament (Fig. 2F). Subsequently, the proximal end of the graft was tied around the lateral head of gastrocnemius (Fig. 2G and H). The lateral head of gastrocnemius was used as a suspensory point for the femoral sling fixation of the graft (Fig. 2I). Finally, with the knee extended, tibial fixation was achieved with sutures (Ethicon 6-0) tied over the anterior bridge of tibia under manual tension and the incision was closed. In Group 5, mice underwent the same ALCR surgical procedures except for a tiny clip fixation but not suture fixation on the femoral side (Fig. 2J) as previously described by Deng *et al* [14].

Micro-CT analysis

The knees were dissected from mice, fixed in 4% paraformaldehyde at room temperature for 24 h and stored in 70% ethanol. After wrapped and fixed on the platform, the specimens were scanned using Skyscan 1176

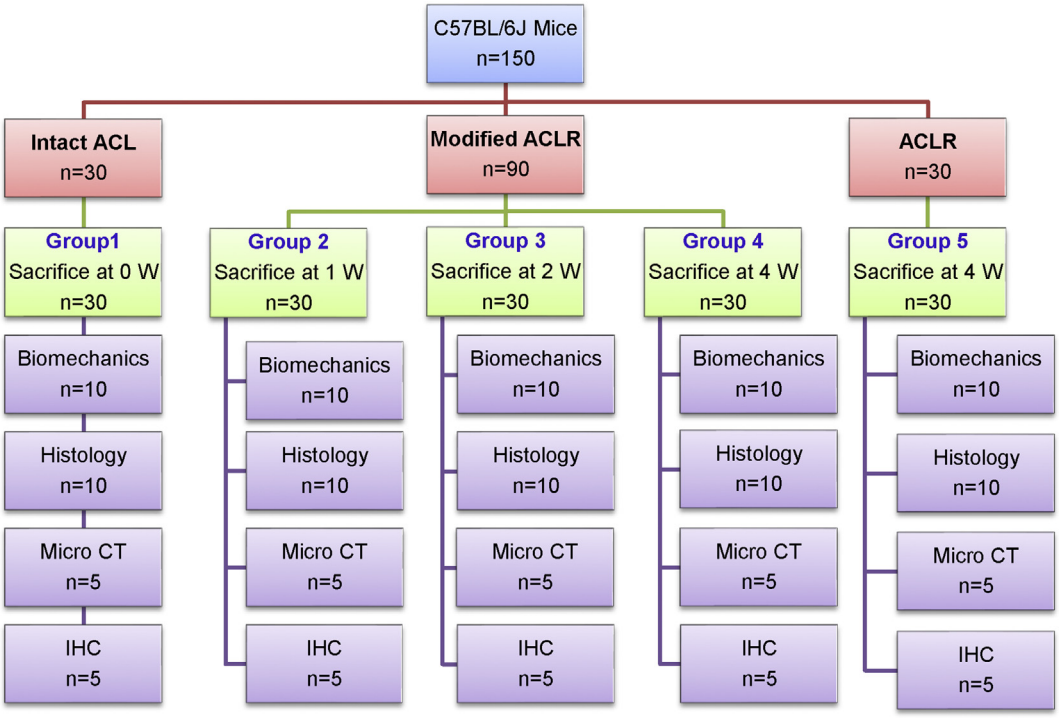

Fig. 1. Diagram of animal treatment and study design of the project.

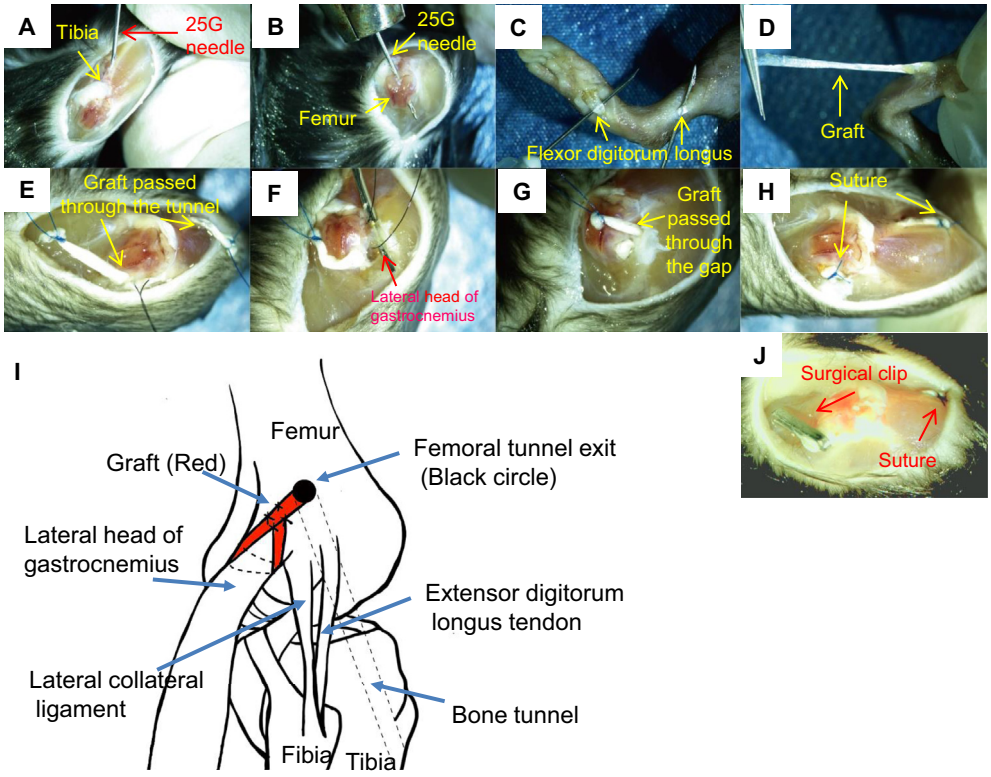

Fig. 2. Murine modified ACLR procedures. (A) Following the exposure of the lateral capsule and ACL of the right knee joint. (B) a bone tunnel is created in the anterior portion of the proximal tibia and lateral femoral condyle using a 25-gauge needle. (C, D) A flexor digitorum longus tendon graft is harvested through a small incision in the leg and the plantar aspect of the foot, respectively. (E) The tendon graft was pulled through the tibial and femoral tunnels in turn. (F) After the exposure of the lateral head of gastrocnemius, (G) the proximal end of the graft passed through the femoral tunnel (H) were further tied around the lateral head of gastrocnemius, while the distal end of the graft was fixed in the tibial side by transosseous suture. (I) Hand drawing illustrates the specific fixation method of graft in the femoral side. (J) Illustration of the primary ALCR model as previously described.

micro-CT machine (Bruker micro-CT N.V., Kontich, Belgium) with following parameters: an isotropic voxel size of 9 μm, a resolution of 4000 × 2672 pixels, 0.2 mm Al, 786 ms, 45 kV, 555 μA, and 0.3 rotation step. Images of each specimen were reconstructed with NRecon software (Skyscan) and the mean distances between several anatomical landmarks were evaluated in DataViewer V.1.4.3 software (SkyScan). To assess the volume and density of newly formed mineralized tissue inside the bone tunnel, the mean bone volume/total volume fraction (BV/TV) and bone mineral density (BMD) of a circular 0.5-mm region of interest within the full-length bone tunnel were analyzed.

Biomechanical tests

The femur-ACL-tibia complex of the knee joint was dissected and all soft tissues were stripped off so that the ACL is the only element connecting the femur and the tibia. Samples were washed clean in phosphate-buffered solution and blotted with filter paper to remove water, followed by coated with bone cement at the proximal and distal end for ease of griping and to prevent the femur and the tibia from damaging by a clamp. With the direction of distraction along the long axis of the ACL graft, a load-to-failure protocol was performed at a strain rate of 10 mm/min on the tensile testing machine (Instron5569, Norwood, MA, USA). The maximal load at failure or pullout (N), stiffness (N/mm), and the site of failure at 2 weeks and 4 weeks post-surgery were well documented.

Histologic staining

Knee joints were harvested and fixed in 4% paraformaldehyde for 24 h. After decalcified with 14% ethylenediaminetetraacetic acid solution for 2 weeks, the specimens were dehydrated through a graded ethanol series and embedded in paraffin, sectioned at 4 μm thickness parallels to the longitudinal axis of the bone tunnel. Hematoxylin and eosin (H&E) and Safranin O staining were performed to analyze changes in histologic structure.

IHC analysis

After deparaffinized, sections were treated with 0.3% hydrogen peroxide to reduce endogenous peroxidase activity. Then antigen retrieval was performed with the sections incubated at 60°C with 0.1 mol/L citrate buffer overnight. Normal goat serum (diluted 1:20) (Invitrogen, MD, USA) was added for 30 min at room temperature to block non-specific staining. Subsequently, the sections were treated with primary antibodies, including Gli2 (1:100), Gli3 (1:100), Smo (1:100), Ptch1 (1:100), Ihh (1:100) (Abcam, MA, USA) and further incubated overnight at 4°C. Secondary biotinylated goat anti-mouse antibody (diluted 1:1000) (Invitrogen, MD, USA) was subsequently added for 30 min incubation the following day. Diaminobenzidine solution (Invitrogen, MD, USA) and followed by counterstaining with hematoxylin was used to detect positive staining of sections. The H-score ranged from 0 to 300 was used for semiquantitative assessment of IHC images according to both the intensity of staining and the percentage of cells stained.

Statistical analysis

All the data are represented as Mean ± SD. Student's *t*-test and one-way ANOVA with Tukey's test was used for pairwise comparisons and multi-Group comparison, respectively. The micro-CT data of the femoral and tibial tunnels and H-scores was compared by Wilcoxon signed-rank test. Statistical analysis was performed with SPSS for Windows, version 19 (SPSS, Inc., Chicago, IL, USA) and GraphPad Prism software (GraphPad Software Inc., La Jolla, CA). $p < 0.05$ was considered to be significant.

Results

All animals tolerated the ACLR procedure without any perioperative complications. They all survived well until they sacrificed.

Micro CT analysis

To investigate whether new bone formation occurs at the tendon-bone interface along with the bone tunnel healing. Micro CT analysis of bone tunnel was performed in Group 3–5, and results showed that no obvious new bone formation was observed at the graft-tunnel interface (Fig. 3A). The bone morphological parameters (BV/TV and BMD) of CT slices were further analyzed by CT An v1.15 software in SkyScan. The median of BV/TV in femoral and tibial tunnels in the Group 3 was 0.035% and 0.033%, respectively, which became 0.063% and 0.059% in the Group 4 and 0.059% and 0.064% in the Group 5 (Fig. 3B). The median of BMD in femoral and tibial tunnels in Group 3 was 0.42 and 0.28 g/cm3, which became 0.65 and 0.57 g/cm3 in the Group 4 and 0.62 and 0.49 g/cm3 in the Group 5 (Fig. 3C). There was a non-significant increase in BV/TV and BMD of the femoral and tibial in Group 4, compared with Group 3 ($n = 5$, $p > 0.05$ for both). And no significant difference in BV/TV and BMD of the femoral and tibial was observed between Group 4 and 5 ($n = 5$, $p > 0.05$ for both).

Biomechanical tests

To determine the changes in the mechanical strength of femur-ACL-tibia complex, load-to-failure tests were performed (Fig. 4A). The mean load-to-failure force in Group 3 and 4 decreased to 31.7% and 46.0% of that in Group 1 (1.82 ± 0.71 N and 2.64 ± 1.20 N *vs* 5.74 ± 1.22 N), respectively. And the mean load-to-failure force in Group 5 was 2.69 N ± 0.90 N (Fig. 4B). Compared with Group 1, significant decreases were observed in Group 3 (mean difference, 3.92 N; 95% CI, 2.73–5.11 N; $p < 0.001$), and 4 (mean difference, 3.10 N; 95% CI, 1.91–4.29 N; $p < 0.001$). Compared with Group 4, no significant difference was observed in Group 3 (mean difference, 0.82 N; 95%CI, −0.37 to 2.01 N; $p > 0.05$), and 5 (mean difference, 0.05 N; 95% CI, −1.30 to 1.20 N; $p > 0.05$).

Subsequently, we calculated the stiffness of graft from the load–deformation curves, and results showed that the graft stiffness of Group 3 and 4 significantly decreased to 33.1% and 57.2% of that in Group 1 (1.66 ± 0.83 N/mm and 2.87 ± 1.55 N/mm *vs* 5.01 ± 1.98 N/mm), respectively. And the mean graft stiffness of Group 5 was 2.93 ± 1.19 N/mm (Fig. 4C). Compared with Group 1, significant

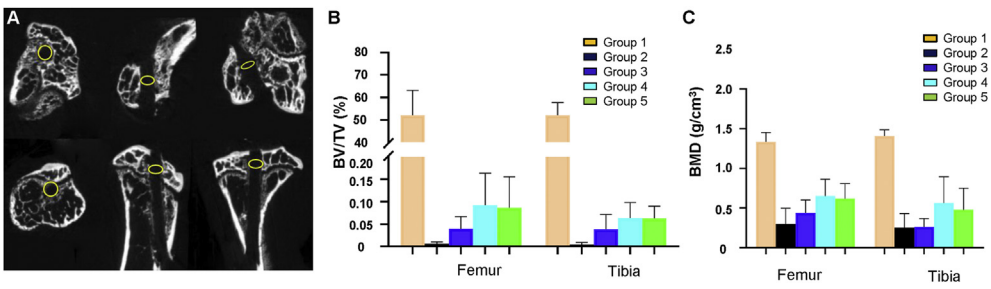

Fig. 3. Micro-CT analysis results. (A) Representative transverse, sagittal and coronal aspects of micro-CT slices of bone tunnel following ACLR. The yellow circle with a diameter of 0.5 mm is equal to the diameter of the needle used to drill the tunnel. (B) Box plots show BV/TV and (C) BMD of newly formed bone in full-length of the femoral and tibial tunnels of mice in Group 3, 4 and 5. The horizontal line is the median, the box represents the first quartile and third quartile, and the bars represent the minimum and maximum. BV/TV, bone volume/total volume fraction; BMD, bone mineral density. (For interpretation of the references to color/colour in this figure legend, the reader is referred to the Web version of this article.)

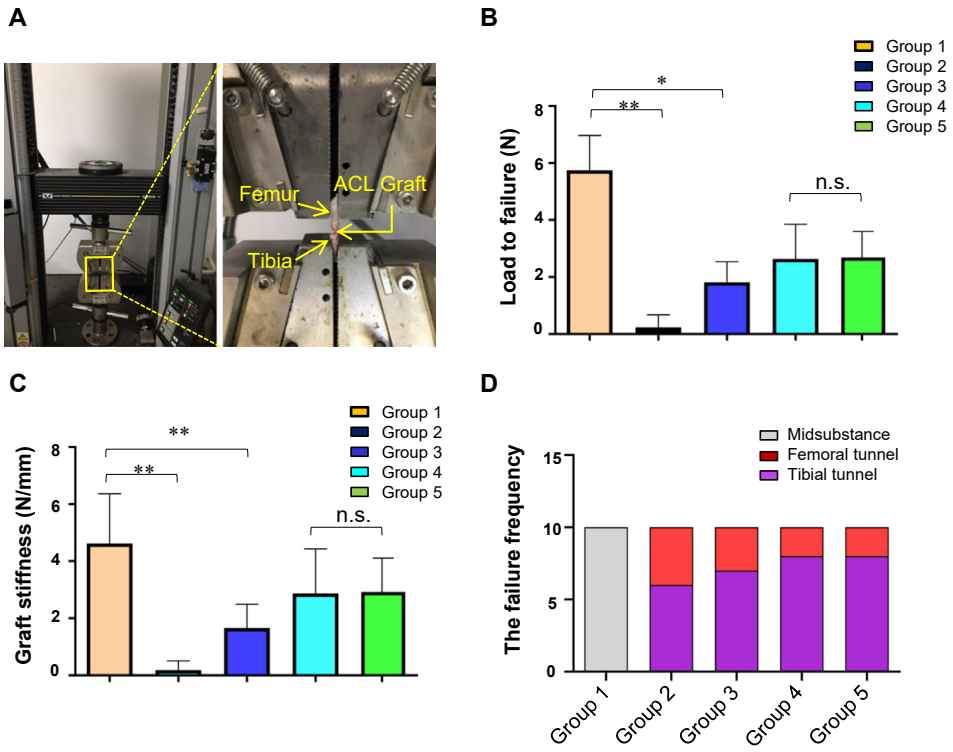

Fig. 4. Biomechanical analysis results. (A) Specimens are fixed into the testing apparatus. The ACL graft or the intact ACL is the only tissue connecting the femur and the tibia. (B) Load-to-failure force and (C) graft stiffness results of mice in Group 1–5. (D) The site of graft failure in Group 1–5. *$p < 0.05$; **$p < 0.01$; n.s., nonsignificant.

decreases were observed in Group 3 (mean difference, 2.97 N; 95%CI, 1.38–4.55 N; $p < 0.001$) and 4 (mean difference, 1.75 N; 95% CI, 0.17–3.34 N; $p < 0.05$). Compared with Group 4, no significant difference was observed in Group 3 (mean difference, 1.21 N; 95% CI, 0.38–2.81 N; $p > 0.05$) and Group 5 (mean difference, 0.05 N; 95% CI, −1.70 to 1.60 N; $p > 0.05$).

The site of graft failure (femoral tunnel, midsubstance, or tibial tunnel) in this study was recorded and we found that all the native ACLs in Group 1 break at the midsubstance during load-to-failure tests, whereas 6 and 4 of the 10 grafts failed at the tibial and the femoral side for the Group 2 as well as 7 and 3 of the 10 grafts failed at the tibial and the femoral side for both the Group 3 and 5, respectively. For Group 4, 8 of the 10 grafts failed at the tibial side, 2 failed at the femoral side in Group (Fig. 4D).

Histologic staining

To evaluate the effect of modified ALCR on the fibrovascular formation in the tibia tunnel, Safranin O staining was conducted with transverse sections of the tibial tunnel in each Group. As shown in

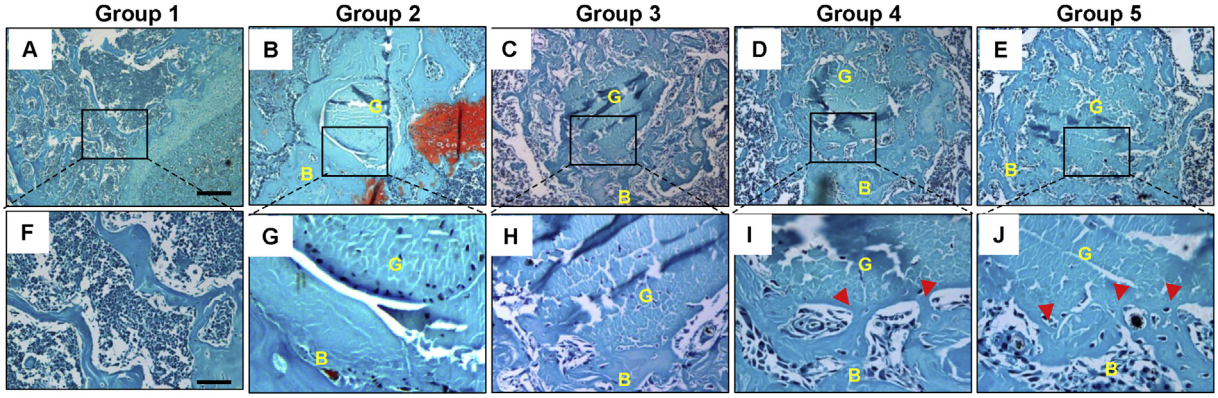

Fig. 5. Histological staining results. (A–J) Safranin O staining results of transverse sections of tibial tunnels in each Group. Normal transverse section of trabecular bone in tibia (A, F). There is no junction observed between graft and tunnel of mice in Group 2 (B, G). No obvious junction forms between graft and tunnel of mice in Group 3 (C, H). And direct junction appeared between tendon graft and the tunnel of mice in Group 4 (D, I) and 5 (E, J). Red arrows in **I** and **J** indicate a direct junction of graft to bone tunnel. Boxed area in A-E is shown at high magnification in F-J, respectively. Scale bars = 200 μm in A-E; Scale bars = 50 μm in F-J. B: bone; G: graft; IF: interface. (For interpretation of the references to color/colour in this figure legend, the reader is referred to the Web version of this article.)

Fig. 5A–J, normal trabecular bone was observed in the proximal of tibia (Fig. 5A, F) and a clear boundary between tendon graft and tunnel in the tibial tunnel near growth plate began to be observed at Group 2 (Fig. 5B, G) and Group 3 (Fig. 5C, H) (initiated 2 weeks after ACLR surgery), and direct junction interfaces were observed in Group 4 (Fig. 5D, I) and Group 5 (Fig. 5E, J) (4 weeks after ALCR surgery), suggesting fibrous connections appeared between tendon graft and tunnel in Group 4 and Group 5.

Similar with the above results from Safranin O staining, H&E staining of normal ACL enthesis showed continuous collagen fibers from ACL to tibial bone in Group 1 (Fig. 6A, F), whereas H&E staining of the tibia tunnel in Group 2–5 also confirmed that formation of disorganized fibrovascular scar-tissues initiates 2 weeks after ALCR surgery, and well-organized graft-tunnel interfaces were observed in Group 4 and 5 (Fig. 6A–J). No significant alterations were observed between Group 4 and 5, which were structurally different from normal ACL enthesis in Group 1 (Fig. 6D and E, I–J). In order to eliminate the possibility that the fibrovascular formation resulted from the activation of growth plate, we further detected the healing status around the aperture of the tibial tunnel. The H&E results showed that similar to the healing occurred in inner of the tibia tunnel, formation of disorganized fibrovascular scar-tissues in the aperture of the tibia tunnel emerged at 2 weeks after ALCR surgery (Fig. 6M, R), and huge amounts of fibrovascular scar-tissues around the aperture of the tibial tunnel were observed at 4 weeks after ALCR surgery Group 4 and 5 (Fig. 6N and O, S and T). No significant alterations were also observed between Group 4 and 5 at the interface in the aperture of the tibia tunnel. The above demonstrated that natural process after ACL reconstruction couldn't achieve the structure of normal ACL enthesis.

IHC analysis

To explore the roles of Hh signaling in graft healing, the expression patterns of key proteins in Hh signaling during the scar-mediated fibrovascular formation were examined by IHC analysis. IHC results of Ihh and its receptor (Ptch1) showed that strong positive expressions of Ihh and Ptch1 were relatively restricted in the graft-tunnel interface in Group 2–4, compared with surrounding tissues. According to the comparison among the Groups, the expression of IHH on the tendon-bone interface gradually decreased with the extension of healing time (Fig. 7A, F). IHC results of Smo and transcription factor Gli2/3 demonstrated that all of them highly expressed at various parts of the tissue. As expected, both Smo and Gli2 on the tendon-bone interface were remarkably increased during the process of graft-tunnel healing (from 1 to 4 weeks after ACLR surgery) (Fig. 7C, D, F). However, Gli3 firstly expressed at various parts of the tissue at Group 1 (1 week after ALCR surgery) and significantly decreased with the extension of healing time (Fig. 7E and F). All these data suggest that Ihh mediated Hh signaling is activated on the tendon-bone interface and may be involved in the process of graft healing after ACLR surgery by increasing Gli2 and reducing Gli3.

IHC results showed no significant difference in the expression of key proteins in Hh signaling between Group 4 and 5 (Fig. 7F). It indicates that our modified surgical model of mice ACLR is successful. In addition, IHC of native ACL enthesis showed positive staining of Ihh, Ptch1, Smo and Gli3 but not Gli2 in Group 1. It explained why scar-mediated natural process after ACLR failed to recover enthesis-like structure. Inconsistent expression patterns of Hh signaling in Groups 4 and 5 compared with ACL enthesis in Group 1 suggest that Hh signaling may be a regulator to

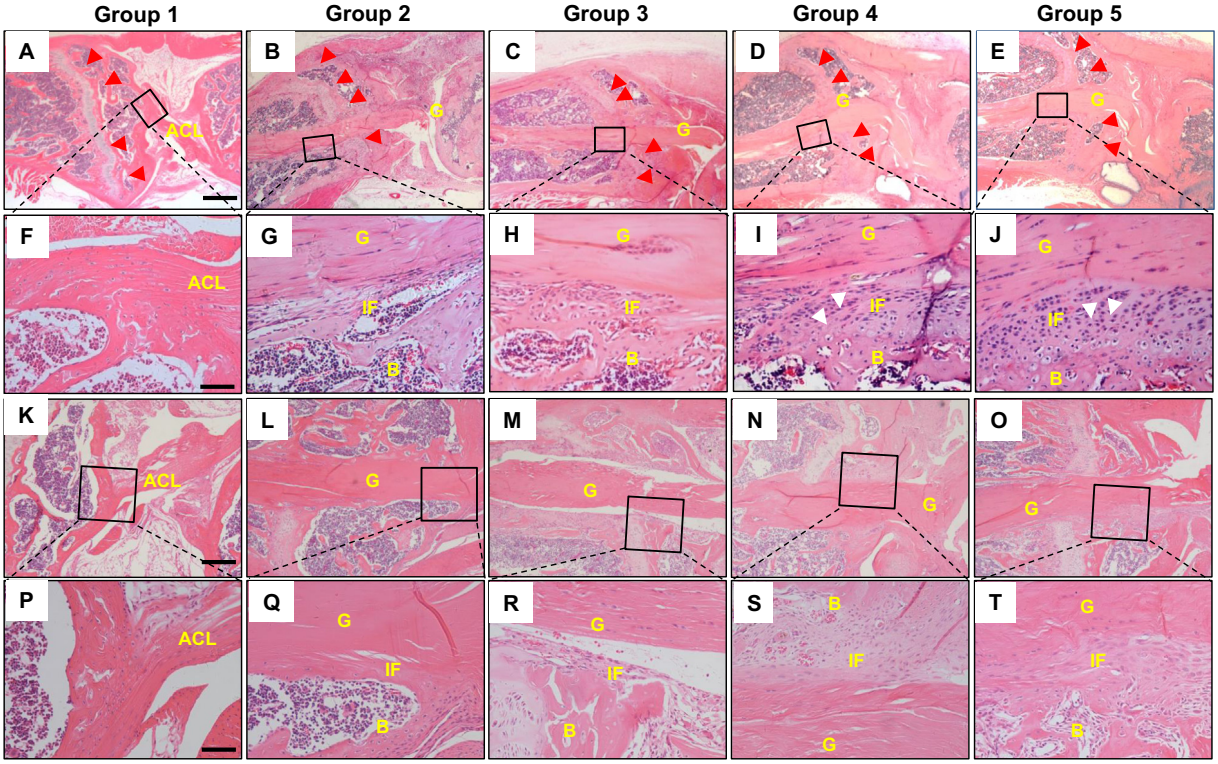

Fig. 6. H&E staining results of tibial tunnel. (A–J) H&E staining results of tibial tunnel near the tibial growth plate of mice knee in each Group. Continuous collagen fibers from ACL to tibial bone were observed in Group 1(A, F). Disorganized fibrovascular granulation tissue formed in Group 3 mice (C, H) and well-organized graft-tunnel interface appeared in Group 4 (D, I) and 5 (E,J). Red arrows in A-E indicate the position of the growth plate. Boxed area in A-E is shown at high magnification in F-J, respectively. (K–T) H&E staining results of bone tunnel near the tibial aperture of mice in each Group. Native enthesis showed continuous collagen fibers connection (K, P). No fibrovascular tissue was seen at the interface in Group 2 (L, Q). Less fibrovascular tissue existed on the tunnel side in Group 3 (M, R). Mass formation of fibrovascular granulation tissue appeared at the tendon-bone interface of mice in Group 4 (N, S) and 5 (O, T). Boxed area with black frame in row 1 and 3 of the illustrations was shown at high magnification in row 2 and 4, respectively. Scale bars = 400 μm in A-E; Scale bars = 200 μm in F-J, P-T; Scale bars = 50 μm in K–O. B, bone; G, graft; IF, interface. (For interpretation of the references to color/colour in this figure legend, the reader is referred to the Web version of this article.)

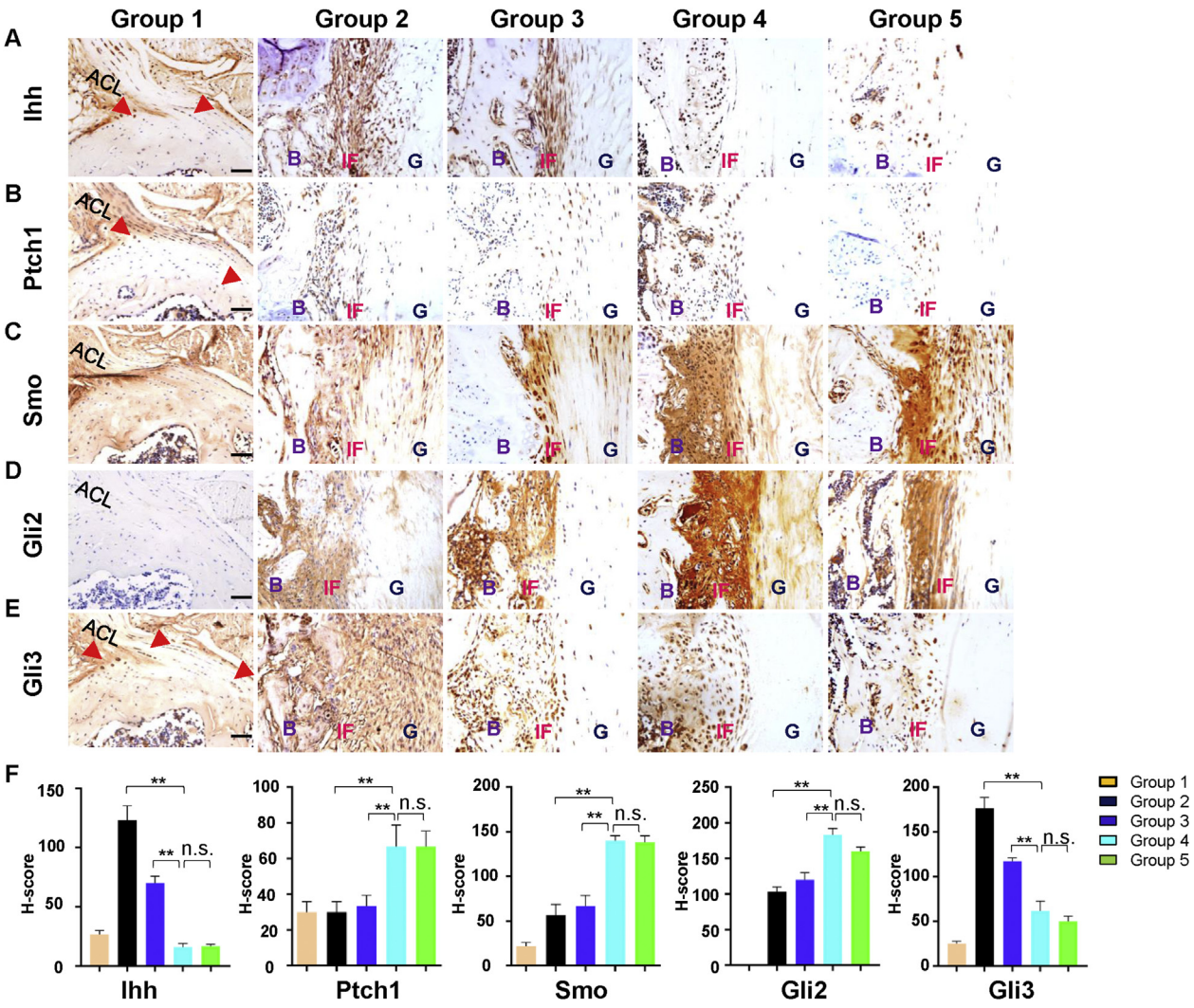

Fig. 7. IHC results of key proteins in Ihh signaling at the tendon-bone interface in Group 1–5 mice. (A–E) Expression of Ihh, Ptch1, Smo, Gli2, Gli3 proteins at the tendon-bone interface. (F) IHC semi-quantitative expression results of key proteins in Ihh signaling using H-score at the tendon-bone interface in Group 1–5 mice. The H-score ranged from 0 to 300 was used for semi-quantitative assessment of IHC images according to both the intensity of staining and the percentage of cells stained. The intensity was considered 0 for absent expression, 1^+ for weak staining, 2^+ for moderate staining, and 3^+ for strong staining. The H-score was calculated as the formula: H-score = 1 × percentage of 1^+ cells +2 × percentage of 2^+ cells +3 × percentage of 3^+ cells. Scale bars = 50 μm. Data are expressed as the Mean ± S.D. $^*p < 0.05$; $^{**}p < 0.01$; n.s. indicates no significant difference.

change the phenotype of scar-mediated fibrovascular formation at tendon-bone interface.

Discussion

ACLR mouse model is an important tool that will enable us to explore the detailed biological processes and molecular events on tendon-bone healing, with hopes of establishing new strategies for promoting healing and putting into clinical practice. In this study, we established and validated a simple, metal-free and reproducible mouse ACLR in the C57BL/6 background. Comparative study on results from micro-CT, biomechanical and histological analysis demonstrated that no significant difference was found between our modified ACLR model and the previous one. We found that the phenotype of a scar-mediated fibrovascular tissue interface emerges between the graft and bone tunnels in our model, which had been reported by previous studies in larger animal models [10,12] and clinical research [11]. Moreover, a large amount of fibrovascular granulation tissue also formed near the aperture of the tibial tunnel, which indicated that the microenvironment in the tibial aperture may be beneficial to graft-tunnel healing. In addition, our data suggested that the activation of Hh signaling on the tendon-bone interface may be involved in the process of graft healing after ACLR surgery by regulating the transcription factors Gli2 and Gli3.

Our biomechanical findings were consistent with the previous report [14], in which a 23-gauge needle (diameter = 0.64 mm) was used for bone tunnel drilling, a tiny surgical clip for suspensory fixation on the femoral side and transosseous suture fixation on the tibial side. They reported a mean failure force of 1.29 ± 0.47 N and 1.79 ± 0.40 N at 2 weeks and 4 weeks after surgery, respectively, whereas we found higher load-to-failure of the native tendon (5.43 ± 0.79 N). This discrepancy could be due to measuring error of different biomechanical devices. Similar to previous studies, load to failure tests showed that a majority of specimens in the ACLR Groups were pulled out from the tibial tunnel, indicating that the tendon-bone interface is the weakest site on the whole femur-ACL-tibia complex [22–24]. Most of the specimens break in the tibial side may demonstrate that the healing quality of the tendon to bone attachment in the femoral side is prior to that in the tibial side. This is consistent with our histological findings and others' reports that they noted poor healing in the tibia after ACLR [25,26].

Previous studies had found new bone formation at the tendon-bone interface along the bone tunnel by micro-CT analysis [14,25]. In this study, we didn't find any noticeable new bone formation at the graft-tunnel interface on micro-CT slices and no difference was found on the increased BV/TV and BMD. This is probably due to the smaller diameter of the needle we use to drill the bone tunnel and the shorter duration of research. Our results indicated that a larger diameter of the bone tunnel might be beneficial to accommodate more newly formed bone.

The Ihh signaling pathway plays a critical role in enthesis development. Previous gain- and loss-of-function studies have indicated hedgehog signaling as a key regulator of ligamental enthesis growth, fibrocartilage differentiation, and calcified cartilaginous mineralization [17,18,27]. In this study, we identified the activation of hedgehog signaling in the tendon-bone interface and significantly increased expression of Ptch1, Smo and Gli2 and decrease expression of Gli3. This finding is similar to a study in a rat ACLR model [27] that Ihh as well as Ptch1 and Gli1, the downstream proteins of Ihh signaling cascade, were positively located at the tendon-bone interface. In addition, the study performed by Zong [28] showed high Gli1, Ptch1 expression and high numbers of Ihh^{+} cells at the enthesis in a rat rotator cuff repair model, which also provided strong evidence that Ihh signaling pathway plays a role in tendon-to-bone healing. Our findings suggested that Ihh signaling pathway might be a key regulator for fibrovascular interface formation after ACLR. According to the expression pattern of Gli2 and Gli3 in the interface of tendon-bone, we speculated that activation of hedgehog signaling in graft-tunnel integration is mediated by increasing activator form of Gli2 cooperates with decreasing repressor form of Gli3. Further studies such as genetic modification of genes (*Smo*, *Gli2* and *Gli3*) in Ihh signaling can further confirm the role of Ihh signaling in graft-to-tunnel healing.

Compared with the previously ACLR murine model [14,15], the advantage of our modified ACLR model is that no metal fixation device was utilized. Given the narrow space of mouse knee joint, it's difficult to accommodate any tiny metal fixation device. Besides, a soft-tissue sling fixation provides a safer and more reliable fixation on the femoral side than a clip-like device. Furthermore, it's easy to find the physiological space of the lateral head of gastrocnemius which is behind the lateral collateral ligament. However, there were several limitations. First, the small size of the mouse knee makes it uneasy to do a surgical model of ACLR. The operator requires not only experience on human ACLR and microsurgical skills but also familiar to the anatomy of mouse knees. Second, it is unclear whether the femoral technique for graft fixation has any impact on the motion of the ipsilateral lower limb of mice. Due to the influence factor of flexor digitorum longus harvest exists, we have not performed a gait analysis. To answer this question, further studies are maybe required to do gait analysis on a mouse model of allograft ACLR. Third, we observed only three time-points and did not assess graft remodeling and reviving, because our purpose was to detect the initial signaling pathway involved in tendon-bone integration.

Conclusions

Collectively, we introduced and validated a metal-free and easy-reproducible mouse model of ACLR that could be utilized to study pathophysiology and molecular mechanisms of graft-tunnel healing. The purpose of this study was to introduce and validate a simple, metal-free and reproducible mouse ACLR model as an effective tool for raising our understanding of the physiology of tendon-bone healing.

Conflict of Interest

The authors have no conflicts of interest to disclose in relation to this article.

Acknowledgements

This study was supported by National Natural Science Foundation of China (81804121, 81973870, 81573994), Natural Science Foundation of Zhejiang Province (LY19H270006, LQ17H270005), China Postdoctoral Science Foundation (2018M632154), Traditional Chinese Medical Administration of Zhejiang Province (2017ZB026), Zhejiang medical and health science and technology project (2018269058), Zhejiang Chinese medical university scientific research fund project (2018ZG20), the Science and technology innovation program for college students (new talent program) of Zhejiang Province (2018R410030), Opening Project of Zhejiang Provincial Preponderant and Characteristic Subject of Key University (Chinese Traditional Medicine), Zhejiang Chinese Medical University (ZYX2018008), Plan Guide Project of HangZhou Technology Department (20171226Y98), Plan technology project of HangZhou Health Department (2018B028).

References

[1] Griffin LY, Albohm MJ, Arendt EA, Bahr R, Beynnon BD, Demaio M, et al. Understanding and preventing noncontact anterior cruciate ligament injuries: a review of the Hunt Valley II meeting, January 2005. Am J Sports Med 2006;34(9):1512–32.
[2] Mather 3rd RC, Koenig L, Kocher MS, Dall TM, Gallo P, Scott DJ, et al. Societal and economic impact of anterior cruciate ligament tears. J Bone Joint Surg Am 2013;95(19):1751–9.
[3] Oiestad BE, Engebretsen L, Storheim K, Risberg MA. Knee osteoarthritis after anterior cruciate ligament injury: a systematic review. Am J Sports Med 2009;37(7):1434–43.
[4] Tibor L, Chan PH, Funahashi TT, Wyatt R, Maletis GB, Inacio MC. Surgical technique trends in primary ACL reconstruction from 2007 to 2014. J Bone Joint Surg Am 2016;98(13):1079–89.
[5] Calejo I, Costa-Almeida R, Gomes ME. Cellular complexity at the interface: challenges in enthesis tissue engineering. Adv Exp Med Biol 2019;1144:71–90 [eng].
[6] Cho NS, Rhee YG. The factors affecting the clinical outcome and integrity of arthroscopically repaired rotator cuff tears of the shoulder. Clin Orthop Surg 2009;1(2):96–104.
[7] Ardern CL, Taylor NF, Feller JA, Webster KE. Fifty-five per cent return to competitive sport following anterior cruciate ligament reconstruction surgery: an updated systematic review and meta-analysis including aspects of physical functioning and contextual factors. Br J Sports Med 2014;48(21):1543–52.
[8] Cinque ME, Dornan GJ, Chahla J, Moatshe G, LaPrade RF. High rates of osteoarthritis develop after anterior cruciate ligament surgery: an analysis of 4108 patients. Am J Sports Med 2018;46(8):2011–9.
[9] Dingenen B, Gokeler A. Optimization of the return-to-sport paradigm after anterior cruciate ligament reconstruction: a critical step back to move forward. Sports Med 2017;47(8):1487–500.
[10] Goradia VK, Rochat MC, Grana WA, Rohrer MD, Prasad HS. Tendon-to-bone healing of a semitendinosus tendon autograft used for ACL reconstruction in a sheep model. Am J Knee Surg 2000;13(3):143–51.
[11] Nebelung W, Becker R, Urbach D, Ropke M, Roessner A. Histological findings of tendon-bone healing following anterior cruciate ligament reconstruction with hamstring grafts. Arch Orthop Trauma Surg 2003;123(4):158–63.
[12] Rodeo SA, Arnoczky SP, Torzilli PA, Hidaka C, Warren RF. Tendon-healing in a bone tunnel. A biomechanical and histological study in the dog. JBJS 1993;75(12):1795–803.
[13] Chen CH. Graft healing in anterior cruciate ligament reconstruction. Sports Med Arthrosc Rehabil Ther Technol 2009;1(1):21.
[14] Deng XH, Lebaschi A, Camp CL, Carballo CB, Coleman NW, Zong J, et al. Expression of signaling molecules involved in embryonic development of the insertion site is inadequate for reformation of the native enthesis: evaluation in a novel murine ACL reconstruction model. J Bone Joint Surg Am 2018;100(15):e102.
[15] Nakagawa Y, Lebaschi AH, Wada S, Green SJE, Wang D, Album ZM, et al. Duration of postoperative immobilization affects MMP activity at the healing graft-bone interface: evaluation in a mouse ACL reconstruction model. J Orthop Res 2019;37(2):325–34.
[16] Alman BA. The role of hedgehog signalling in skeletal health and disease. Nat Rev Rheumatol 2015;11(9):552–60.
[17] Breidenbach AP, Aschbacher-Smith L, Lu Y, Dyment NA, Liu CF, Liu H, et al. Ablating hedgehog signaling in tenocytes during development impairs biomechanics and matrix organization of the adult murine patellar tendon enthesis. J Orthop Res 2015;33(8):1142–51.
[18] Schwartz AG, Long F, Thomopoulos S. Enthesis fibrocartilage cells originate from a population of Hedgehog-responsive cells modulated by the loading environment. Development 2015;142(1):196–206.
[19] Lim CH, Sun Q, Ratti K, Lee SH, Zheng Y, Takeo M, et al. Hedgehog stimulates hair follicle neogenesis by creating inductive dermis during murine skin wound healing. Nat Commun 2018;9(1):4903.

[20] Kilkenny C, Browne WJ, Cuthill IC, Emerson M, Altman DG. Improving bioscience research reporting: the ARRIVE guidelines for reporting animal research. PLoS Biol 2010;8(6):e1000412.
[21] Council NR. Guide for the Care and use of laboratory animals. 1996. http://newton.nap.edu/html/labrats/.
[22] Bedi A, Kovacevic D, Fox AJ, Imhauser CW, Stasiak M, Packer J, et al. Effect of early and delayed mechanical loading on tendon-to-bone healing after anterior cruciate ligament reconstruction. J Bone Jt Surg Am 2010;92(14):2387.
[23] Kanaya A, Deie M, Adachi N, Nishimori M, Yanada S, Ochi M. Intra-articular injection of mesenchymal stromal cells in partially torn anterior cruciate ligaments in a rat model. Arthroscopy 2007;23(6):610–7.
[24] Rodeo SA, Voigt C, Ma R, Solic J, Stasiak M, Ju X, et al. Use of a new model allowing controlled uniaxial loading to evaluate tendon healing in a bone tunnel. J Orthop Res 2016;34(5):852–9.
[25] Lui PPY, Ho G, Shum WT, Lee YW, Ho PY, Lo WN, et al. Inferior tendon graft to bone tunnel healing at the tibia compared to that at the femur after anterior cruciate ligament reconstruction. J Orthop Sci 2010;15(3):389–401.
[26] Wen C-Y, Qin L, Lee K-M, Wong MW-N, Chan K-M. Grafted tendon healing in tibial tunnel is inferior to healing in femoral tunnel after anterior cruciate ligament reconstruction: a histomorphometric study in rabbits. Arthrosc J Arthrosc Relat Surg 2010;26(1):58–66.
[27] Carbone A, Carballo C, Ma R, Wang H, Deng X, Dahia C, et al. Indian hedgehog signaling and the role of graft tension in tendon-to-bone healing: evaluation in a rat ACL reconstruction model. J Orthop Res 2016;34(4):641–9.
[28] Zong J-C, Mosca MJ, Degen RM, Lebaschi A, Carballo C, Carbone A, et al. Involvement of Indian hedgehog signaling in mesenchymal stem cell–augmented rotator cuff tendon repair in an athymic rat model. J Shoulder Elbow Surg 2017;26(4):580–8.